# Weak localization and conductance fluctuations in complex mesoscopic geometries

V. Chandrasekhar
*Department of Applied Physics, Yale University, New Haven, Connecticut 06520*
*and IBM Research Division, Thomas J. Watson Research Center, Yorktown Heights, New York 10598*

P. Santhanam
*IBM Research Division, Thomas J. Watson Research Center, Yorktown Heights, New York 10598*

D. E. Prober
*Department of Applied Physics, Yale University, New Haven, Connecticut 06520*
(Received 13 March 1991)

We extend the theory of weak localization and conductance fluctuations in mesoscopic samples to more complex measurement-probe configurations using the network formalism of Douçot and Rammal. Large measurement probes reduce both the amplitude of the localization contribution and the characteristic field scale of the low-field magnetoresistance. We present a simple and physically intuitive picture to explain these results. Our calculations on the length dependence of the conductance fluctuations for wires with narrow measurement probes agree with previous theoretical work, but allow us to make predictions for samples with more complex probe geometries. Furthermore, the detailed shape of the field autocorrelation function is strongly dependent on the geometry of the probes, reminiscent of the weak-localization magnetoresistance. The results of our experiments on weak localization and conductance fluctuations in short Ag wires confirm many of these predictions. We also discuss the relevance of our calculations for the determination of important microscopic parameters such as the electron phase coherence length.

## I. INTRODUCTION

In the past few years, there has been a great deal of interest in the effect of measurement probes on the electrical transport properties of samples whose size is less than or comparable to the electron phase coherence length $l_\phi$, samples in the "mesoscopic" size regime.[1,2] This interest was initiated by two specific results from experiments on conductance fluctuations in mesoscopic samples that were completely unexpected from experiments on macroscopic samples. First, the amplitude of conductance fluctuations in mesoscopic samples was found[3,4] to be much larger than the "universal" value of $\simeq e^2/h$ predicted by Altshuler[5] and by Lee and Stone.[6] Second, the magnetoconductance of such samples was found to be asymmetric in the magnetic field.[7] These experimental results led to a flurry of theoretical activity[8–14] aimed at extending the theory of conductance fluctuations to include the effect of multiple measurement probes. These theories have proved remarkably successful in explaining the qualitative behavior seen in mesoscopic samples. From the point of view of an experimentalist, however, there are still two problems that make a detailed *quantitative* comparison of theory to experiment difficult. First, all of the multiprobe theories of conductance fluctuations mentioned above deal only with samples having probes which are quasi-one-dimensional (1D) with respect to $l_\phi$. In fact, in most of the theories, the probes are assumed to be of the same width as the sample itself. Experimentally, however, the design of measurement probes is more often dictated by lithographic considerations: the probes are usually wider than the sample, and may even be two-dimensional (2D) with respect to $l_\phi$. As we shall show in this paper, the presence of wide probes can have a large effect on the measured properties of the sample. Second, for a quantitative comparison to theory, one must be able to reliably determine important scattering lengths such as $l_\phi$, the spin-orbit scattering length $l_{so}$, and the magnetic impurity scattering length $l_s$. In a normal metal, the simplest (and quite frequently the only) means available to infer these scattering lengths is to fit the low-field magnetoresistance to the standard theory[15,16] of weak localization, which does not take into account the effect of measurement probes. For macroscopic samples such as thin films and long wires, this works remarkably well. For mesoscopic samples, where the standard theory is no longer adequate, a mesoscopic theory of weak localization is required.

Both problems mentioned above were encountered in some of the early studies on the Aharonov-Bohm effect in single Al loops.[17] These problems are illustrated in Fig. 1, which shows the magnetoresistance (MR) data for a 1-$\mu$m Al loop at 2.0 K. Also shown is the best fit to the weak-localization theory of Altshuler, Aronov, and Spivak (AAS),[18] which does not take into account the effect of measurement probes. It is clear that the theory does not quantitatively describe the low-magnetic-field data of this loop. The shape of the low-field magnetoresistance curve cannot be fit with the AAS theory. Furthermore, the amplitude of the magnetoresistance is

 

smaller than expected, so that, if one insists on fitting the data to the AAS theory, the values of $l_\phi$ inferred are shorter than those obtained from previous studies on longer 1D wires. At the time these experiments were done, the effect of measurement probes on quantum interference was not fully understood. Experiments on loops of different sizes, however, did indicate that the problem was more acute in the smaller loops, when the loop perimeter was less than $l_\phi$.

These experimental results on single metal loops led us to investigate the simpler case of weak localization in single short metal wires. In order to systematically study the effect of measurement probes, we measured[19] short Ag wires of different lengths and with different measurement probe configurations. As in the case of the metal loops, it was found that the presence of the measurement probes affected both the shape and the magnitude of the weak-localization magnetoresistance. To describe these results quantitatively, we extended the theory of weak localization to include the specific geometry of the probes, and found excellent agreement with experiment. In this paper, we give a detailed derivation of these results, showing how the measurement probes affect both the magnitude and shape of the weak-localization MR. We shall also apply the formalism we develop to calculate conductance fluctuations in short wires with both 1D and 2D probes. As in the case of weak localization, we find that the measurement probes affect the magnitude and shape of the autocorrelation function of the conductance fluctuation, the quantity analogous to the weak-localization MR. Finally, we give more details of our experiments on short Ag wires, presenting some data on conductance fluctuations in short Ag wires with different measurement probe configurations, and discuss some recent experiments on conductance fluctuations performed by other groups.

## II. THEORY OF QUANTUM CORRECTIONS TO THE RESISTANCE

We begin by deriving an expression for the change in the resistance of a short wire due to quantum corrections to the conductivity. The treatment here follows closely the ones given by Maekawa, Isawa, and Ebisawa[10] and by Kane, Lee, and DiVincenzo,[12] which we have generalized to take into account the effects of probes of different dimensions.

The geometry we assume for this calculation is shown in Fig. 2: it consists of a short wire of length $L$ and width $W$ with one current and one voltage probe attached at each end, enabling measurements using the conventional four-probe method. In what follows, we call the region between the voltage contacts the "sample" (labeled $s$ in Fig. 2) and the region outside the voltage contacts the "probes". The probes can be either 1D or 2D with respect to $l_\phi$. (We shall discuss specific cases relevant to our experiment later in this paper.) The probes are attached to ideal conductors at the points $a$, $b$, $c$, and $d$. A constant current $I$ is applied between $c$ and $d$ and the voltage $V$ is measured across $a$ and $b$. Since the total current $I$ across any cross section of the sample is constant, the differential change $\Delta I$ must be zero,

$$\Delta I = \Delta \int dS_\alpha \mathbf{j}_\alpha(r) = \Delta \int dS_\alpha d^3r' \sigma_{\alpha\beta}(\mathbf{r},\mathbf{r}') \mathbf{E}_\beta(\mathbf{r}') = 0 \ . \tag{1}$$

Here $\mathbf{j}_\alpha(r)$ is the current density, $\sigma_{\alpha\beta}(\mathbf{r},\mathbf{r}')$ is the conductivity, and $\mathbf{E}_\beta(\mathbf{r}')$ is the electric field. Expanding the differential, we obtain

$$\Delta \int dS_\alpha d^3r' [\langle \sigma_{\alpha\beta}(\mathbf{r},\mathbf{r}') \rangle \Delta \mathbf{E}_\beta(\mathbf{r}') + \Delta\sigma_{\alpha\beta}(\mathbf{r},\mathbf{r}') \langle \mathbf{E}_\beta(\mathbf{r}') \rangle] = 0 \ , \tag{2}$$

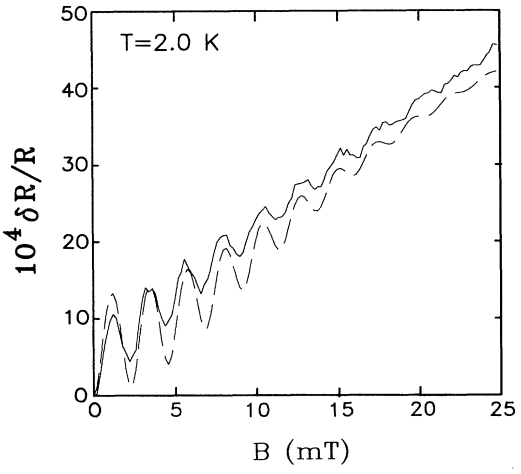


FIG. 1. Low-field magnetoresistance of an approximately 1-$\mu$m square Al loop at 2.0 K. Solid line, data; dashed line, best fit to the isolated loop theory of Altshuler, Aronov, and Spivak with the fitting parameters $l_\phi = 1.2\ \mu$m, $l_{so} = 0.45\ \mu$m.

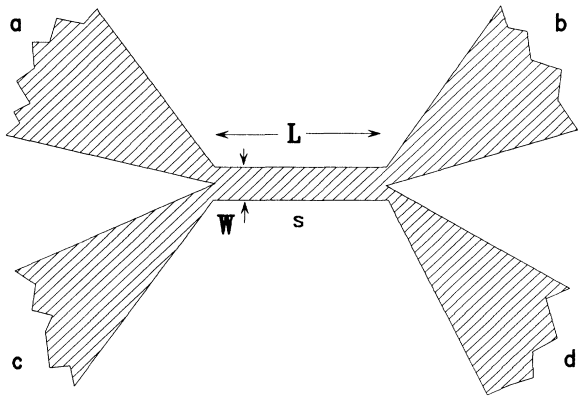


FIG. 2. Schematic of a four-probe measurement of a wire of length $L$ and width $W$. Current is introduced through the probes $c$ and $d$, and the voltage resulting is measured across probes $a$ and $b$.

where we have replaced $\sigma_{\alpha\beta}(\mathbf{r},\mathbf{r}')$ and $\mathbf{E}_\beta(\mathbf{r}')$ by their average values. Following Maekawa, Isawa, and Ebisawa[10] we set $\langle\sigma_{\alpha\beta}(\mathbf{r},\mathbf{r}')\rangle=\sigma_0\delta_{\alpha\beta}\delta(\mathbf{r}-\mathbf{r}')$, where $\sigma_0$ is the classical Drude conductivity. This gives

$$\sigma_0\int dS_\alpha\Delta E_\alpha(\mathbf{r})=-\int dS_\alpha d^3r'\Delta\sigma_{\alpha\beta}(\mathbf{r},\mathbf{r}')\langle\mathbf{E}_\beta(\mathbf{r}')\rangle\ . \quad (3)$$

Now the change in the voltage $\Delta V$ between the points $a$ and $b$ is just given by the line integral of $\Delta E(r)$ between $a$ and $b$. Due to the conservative nature of the electric field, this voltage does not depend on the components of $\Delta E$ perpendicular to the path of integration. Thus it is convenient to calculate the voltage in terms of an electric field averaged over the cross section

$$\Delta E(r)=\frac{1}{S(r)}\int dS\,\Delta E(\mathbf{r})\ ,$$

where $r$ now refers to the coordinate along the path of integration and $S(r)$ is the cross-sectional area perpendicular to $r$. Introducing the notation $\Delta V_{ab,cd}$ as in Ref. 7 of the voltage measured between the points $a$ and $b$ when the current is applied between the points $c$ and $d$, we have

$$\Delta V_{ab,cd}=-\frac{1}{\sigma_0}\int_a^b\frac{dr}{S_\alpha(r)}\int dS_\alpha\int_c^d d^3r'\Delta\sigma_{\alpha\beta}(\mathbf{r},\mathbf{r}')\times\langle\mathbf{E}_\beta(\mathbf{r}')\rangle\ , \quad (4)$$

where, from the notation, it is clear that the integral over $r$ is a line integral.

Kane, Lee, and DiVincenzo[12] have pointed out that setting $\langle\sigma_{\alpha\beta}(\mathbf{r},\mathbf{r}')\rangle=\sigma_0\delta_{\alpha\beta}\delta(\mathbf{r}-\mathbf{r}')$ ignores the long-range contribution to the average conductivity. However, they note that by introducing the classical electric field $\mathbf{E}^{\rm cl}(\mathbf{r})$ in place of the true electric field $\mathbf{E}(\mathbf{r})$ and by applying the appropriate boundary conditions to the long-range part of $\langle\sigma_{\alpha\beta}(\mathbf{r},\mathbf{r}')\rangle$, one obtains Eq. (4) with $\langle\mathbf{E}(\mathbf{r}')\rangle$ replaced by $\mathbf{E}^{\rm cl}(\mathbf{r}')$. The classical field $\mathbf{E}^{\rm cl}(\mathbf{r})$ is nonzero only in the path between the current probes $c$ and $d$, where it is equal to $\mathbf{j}^{\rm cl}(\mathbf{r})/\sigma_0$. Thus the integral over $\mathbf{r}'$ in Eq. (4) has a contribution only when $\mathbf{r}'$ is in the classical current path, i.e., when $\mathbf{r}'$ is on the direct path between the points $c$ and $d$. Equation (4) allows us to determine the change in voltage $\Delta V_{ab,cd}$ given the change in the conductivity $\sigma$.

### A. Weak localization

The weak-localization contribution to the conductivity is given by[15,16]

$$\Delta\sigma^{\rm loc}(r,r')=-\frac{2e^2D}{\pi}C(\mathbf{r},\mathbf{r}')\delta(\mathbf{r}-\mathbf{r}')\ , \quad (5)$$

where $C(\mathbf{r},\mathbf{r}')$, the particle-particle propagator, is the solution of the diffusion equation

$$\left[\left[-i\nabla-\frac{2e\,\mathbf{A}}{\hbar}\right]^2+\frac{1}{l_\phi^2}\right]C(\mathbf{r},\mathbf{r}')=\frac{\delta(\mathbf{r}-\mathbf{r}')}{\hbar D}\ . \quad (6)$$

Here $D=\frac{1}{3}v_F l$ is the electron diffusion constant, $v_F$ being the Fermi velocity and $l$ the elastic mean free path, and $\mathbf{A}$ is the magnetic vector potential. The boundary condition on an insulating boundary is given by

$$\left[-i\nabla_n-\frac{2e\,\mathbf{A}_n}{\hbar}\right]C(\mathbf{r},\mathbf{r}')=0\ , \quad (7)$$

where $\nabla_n$ and $\mathbf{A}_n$ are the components of the appropriate vectors normal to the surface. Physically, this is just the condition that at an insulating boundary, there can be no current normal to the surface. In order to simplify matters, we impose the additional boundary condition that $C(r,r')=0$ at the ends of the wire which are connected to the current an voltage contacts (at $a$, $b$, $c$, and $d$ in Fig. 2), although this assumption is not necessary. Putting Eq. (5) into Eq. (4) we obtain

$$\Delta V^{\rm loc}=\frac{2e^2D}{\pi\sigma_0}\int_L\frac{dr}{S_\alpha(r)}\int dS_\alpha C(\mathbf{r},\mathbf{r})\mathbf{E}^{\rm cl}(\mathbf{r})\ , \quad (8)$$

where the notation makes it clear that the integral over the variable $r$ is performed only over the length $L$ common to both the current and voltage paths. It is important to note that, because of this, the weak-localization contribution is independent of precisely which leads are being used for current and voltage, provided that the length $L$ of the lithographically defined sample remains the same. Thus, if instead of the present configuration we were to use lead $c$ as a voltage lead and lead $b$ as a current lead, we expect the measured weak-localization contribution to remain unchanged.

For the configuration shown in Fig. 2, the region $L$ has a constant area of cross section $A$, and we can then set $E^{\rm cl}(\mathbf{r})=I/\sigma_0 A$. Writing Eq. (8) in terms of the resistance $R=L/\sigma_0 A$, with $\Delta R=\Delta V/I$, we obtain the well-known equation for the weak-localization contribution of a narrow wire[20]

$$\left[\frac{\Delta R}{R}\right]^{\rm loc}=\frac{2e^2D}{\pi\sigma_0 L}\int_L dr\,C(\mathbf{r},\mathbf{r})\ . \quad (9)$$

#### 1. *General formula for a wire*

With Eq. (9), we have, at least conceptually, a simple recipe to determine the weak-localization correction for any 1D sample: solve Eq. (6) with boundary conditions appropriate to the sample geometry and put the result into Eq. (9). In practice, the solution of Eq. (6) for arbitrary sample geometry is not trivial, and an analytical solution can be found for only the simplest cases. In what follows, we shall generalize the network formalism of Douçot and Rammal,[21] who derived the localization correction for a network of 1D wires, to find the solution to these equations.

Consider then the 1D wire of length $L$ and width $W$ with four measurement probes shown in Fig. 3(a). To be definite, we have chosen a configuration with one 2D probe and one 1D probe on either end of the wire; however, the discussion that follows could be applied to wires with any combination of 1D and 2D probes. We shall initially work in zero magnetic field, generalizing the result later to finite field.

For the 1D wire, $C(r,r')$ in the wire depends only on

the coordinates $x$ and $x'$ along the wire, so we shall drop the remaining coordinates in the following discussion and denote it by $C(x,x')$. Let $C_a$ be the value of $C(x,x')$ at one end of the short wire ($x=0$), $C_b$ the value at the other end ($x=L$), and $C_0$ the value at the point $x'$, which is somewhere in the middle of the wire. Between $x=0$ and $x'$, $C(x,x')$ obeys the homogeneous 1D equation

$$\left[-\frac{d^2}{dx^2}+\frac{1}{l_\phi^2}\right]C(x,x')=0 . \tag{10}$$

The solution of this equation is[21]

$$C(x,x')=C_a\cosh(x/l_\phi) + [C_0-C_a\cosh(x'/l_\phi)]\frac{\sinh(x/l_\phi)}{\sinh(x'/l_\phi)} . \tag{11}$$

A similar solution can be found for the strand between $x=x'$ and $L$, and for the two 1D probes on either end of the wire. Equation (11) gives $C(x,x')$ in terms of $C_a$ and $C_b$, which are still unknown and must be determined by the boundary conditions at $x=0$ and $L$. The appropriate boundary condition can be determined by integrating the diffusion equation over a very small volume $v$ around the point $r$

$$\int_v\left[-\nabla\cdot\nabla+\frac{1}{l_\phi^2}\right]C(r,r)d^3r=\frac{1}{\hbar D}\int d^3r\,\delta(\mathbf{r}-\mathbf{r}') . \tag{12}$$

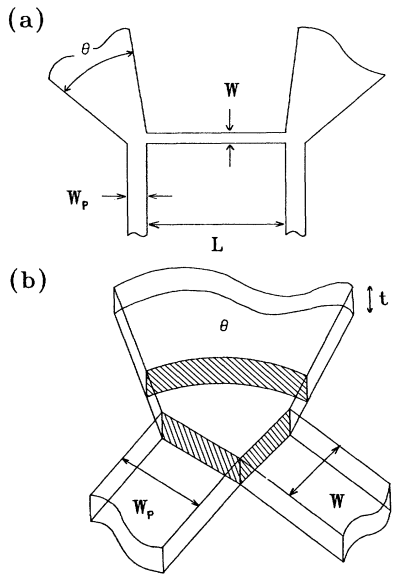


FIG. 3. (a) Geometry assumed for the calculation of the weak-localization contribution of a wire of length $L$ and width $W$. Current is introduced through the two two-dimensional probes which each subtend an angle $\theta$, and voltage is measured across the two one-dimensional probes of width $W_p$. (b) Exploded view of one end of the wire, showing the juncture of the wire, the one-dimensional probe, and the two-dimensional probe.

The first term under the integral sign can be converted by the divergence theorem into a surface integral. The second term can be neglected if the volume of integration $v$ is small in comparison to $l_\phi^2 t$ ($t$ is the thickness of the film). The volume of integration can be always be chosen to satisfy this condition. For example, for the short wire of Fig. 3(b), with one 2D probe and one 1D probe (of width $W_p$) on each end, the maximum volume of the integration region is $W_p Wt$. Thus, when $W$ and $W_p \ll l_\phi$, the second term can be neglected. The term on the right-hand side is zero if the region of integration does not contain $r'$, and unity if it does. Equation (12) then becomes

$$-\int_s \nabla C(r,r')d^2r=\frac{1}{\hbar D}\delta_{r,r'} , \tag{13}$$

where the surface $s$ encloses the volume $v$. Since the boundary condition Eq. (7) still holds for the component of the gradient perpendicular to the surface of the metal, the only contribution to the integral in Eq. (13) is from the component within the plane for the 2D film, and along the 1D strands for the wires.

We now apply Eq. (13) at the point $x=0$, the juncture of the wire, the 1D probe, and the 2D film. The surface of integration is shown in Fig. 3(b). The only contribution to the integral comes from the three regions of the surface which are shaded. The first is in the 2D film, and is part of the surface of a right circular cylinder of radius $r$ and height $t$. Over this surface, the gradient of $C(\mathbf{r},\mathbf{r}')$ is constant and has the value (see Appendix) $-(C_a/r)/[\ln(2l_{\phi 2D}/l)]$, where $l_{\phi 2D}$ is the phase breaking length in the 2D film, which can be different from $l_\phi$ in the 1D wire.[22] Integrating over this region of the surface then gives $-\theta t C_a/[\ln(2l_{\phi 2D}/l)]$, where $\theta$ is the angle subtended by the 2D probe. The value of $C(\mathbf{r},\mathbf{r}')$ over the two other regions in the 1D strands can be calculated from Eq. (11). As before, $\nabla C(\mathbf{r},\mathbf{r}')$ is constant over each of the two regions, and the surface integral just gives the surface areas of each region, which are $Wt$ and $W_p t$ for the wire and the probe, respectively. Noting that the right-hand side of Eq. (13) is zero for the particular volume of integration (since it does not contain $r'$), we obtain, after a bit of algebra,

$$-C_a\eta+\alpha\left[\frac{C_0}{\sinh(x')}-C_a\coth(x')\right]=0 , \tag{14a}$$

where $\eta=\eta_1+\eta_2$, $\eta_2=\theta/[\ln(2l_{\phi 2D}/l)]$, $\eta_1=W_p/l_\phi$, $\alpha=W/l_\phi$, and, to save space, the arguments of the hyperbolic functions are written with respect to $l_\phi$. This equation is the equivalent of the network equations of Douçot and Rammal, generalized to take into account 2D components and 1D strands of different widths. Following Douçot and Rammal, we call the small volume of integration a "node." Two other equations are obtained from the nodes at $x=x'$ and $L$,

$$C_0[\coth(x')+\coth(L-x')]-\frac{C_a}{\sinh(x')} -\frac{C_b}{\sinh(L-x')}=\frac{l_\phi}{\hbar D t W} \tag{14b}$$

and

$$-C_b\eta+\alpha\left[\frac{C_0}{\sinh(L-x')}-C_a\coth(L-x')\right]=0\ . \quad (14c)$$

Equations (14) are three equations which can be solved for the three unknowns $C_a$, $C_0$, and $C_b$. Knowing these, we can determine $C(x,x')$ anywhere in the wire, using Eq. (11). In general, one can write such network equations for geometries with any number of nodes. For $N$ nodes (including the source node at $x'$), we need to solve $N$ linear equations in $N$ unknowns. In complicated geometries, this may not be possible to do in closed form.

Putting $C(x,x')$ into Eq. (9), we obtain our final result for the fractional change in resistance due to weak localization[19]

$$\frac{\Delta R}{R}=\frac{R_\square}{(\pi\hbar/e^2)}\frac{l_\phi}{W}\times\left[\frac{(\eta^2+\alpha^2)\coth L-(l_\phi/L)(\eta^2-\alpha^2)+2\alpha\eta}{\eta^2+\alpha^2+2\alpha\eta\coth L}\right], \quad (15)$$

where $R_\square=(1/\sigma_0 t)$ is the sheet resistance of the wire and $\pi\hbar/e^2\simeq 12.9$ kΩ. Equation (15) gives the weak-localization contribution for a 1D wire with *any* probe configuration. Different probe configurations only change the value of $\eta$; Eq. (15) remains valid.

Before discussing specific geometries, it is useful to consider some general limits of Eq. (15). For the case of a very long wire ($L\gg l_\phi$), Eq. (15) reduces to the familiar result[16]

$$\frac{\Delta R}{R}=\frac{R_\square}{(\pi\hbar/e^2)}\frac{l_\phi}{W}=\frac{R_\square}{(\pi\hbar/e^2)}\frac{1}{\alpha}\ , \quad (16)$$

independent of $\eta$ as we should expect, since the probes should not make any difference. For the short wire ($L\ll l_\phi$), Eq. (15) gives

$$\frac{\Delta R}{R}=\frac{R_\square}{(\pi\hbar/e^2)}\frac{1}{\eta}\ . \quad (17)$$

It should be noted that this has the same form as Eq. (16), with $\alpha$ replaced by $\eta$. This result is independent of the geometry of the wire, depending only on the geometry of the probes through $\eta$. Thus, in this limit, *the weak-localization contribution of the short wire is completely determined by its probes.*

### 2. Dependence on magnetic field

Up to this point, we have not discussed the effect of a finite magnetic field $B$. The magnetic field is usually included in the weak-localization problem through the vector potential in Eq. (6). For the case of 1D wires, it is well known that the effect of a magnetic field can be included by introducing a field-dependent phase coherence length $l_\phi(B)$ defined by[23]

$$\frac{1}{l_\phi^2(B)}=\frac{1}{l_\phi^2}+\frac{1}{3}\left[\frac{\pi WB}{\Phi_s}\right]^2, \quad (18)$$

where $\Phi_s=h/2e$ is the superconducting flux quantum. For 1D probes of width $W_p$, the same equation holds, with $W$ replaced by $W_p$. For 2D probes, it is shown in the Appendix that the effect of a magnetic field is to replace the parameter $\eta_2$ with the field-dependent quantity

$$\eta_2(B)=-2\theta/[\ln(B/4B_0)+\psi(\tfrac{1}{2}+B_\phi/B)]\ , \quad (19)$$

where $\psi$ is the digamma function, $B_0=\hbar/4el^2$ and $B_\phi=\hbar/4el_{\phi 2D}^2$.

In a finite magnetic field, Eq. (15) still remains valid: one just has to replace the parameters $l_\phi$, $\alpha$, $\eta_1$, and $\eta_2$ by their corresponding field-dependent quantities $l_\phi(B)$, $\alpha(B)=W/l_\phi(B)$, $\eta_1(B)=W_p/l_{\phi p}(B)$, and $\eta_2(B)$ as defined in Eq. (19) above.

### 3. Specific probe configurations

The only way the probes enter Eq. (15) is through the parameter $\eta$; different probe configurations correspond to different values of $\eta$. Thus, to determine the formula appropriate for a particular probe configuration, one needs to calculate the parameter $\eta$ appropriate for that configuration. We shall calculate $\eta$ for three specific probe configurations relevant to our experiment; the procedure, however, can be applied to any general probe configuration consisting of 1D and 2D elements. The configurations we shall discuss are shown schematically in Fig. 4. The first [Fig. 4(a)], which we denote the

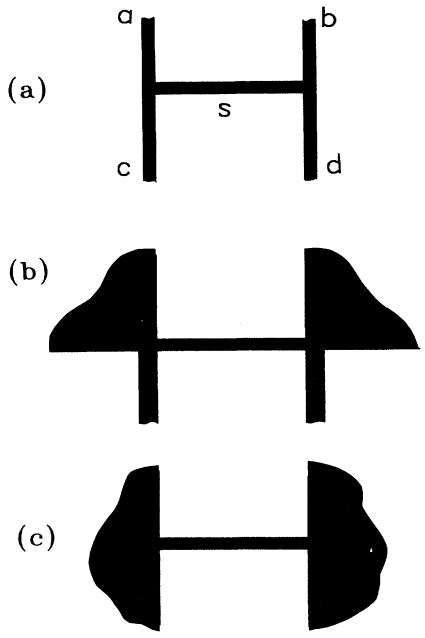


FIG. 4. One-dimensional wires with different probe configurations. (a) Narrow-probes configuration, a wire with four one-dimensional probes of width $W_p\ll l_\phi$. (b) Wide-probes configuration, a wire with two one-dimensional probes and two two-dimensional probes. (c) Wire with only two two-dimensional probes.

"narrow-probes" configuration, is a short wire with four 1D probes of width $W_p < l_\phi$, the standard four-terminal geometry. The second "wide-probes" configuration [Fig. 4(b)] has two 2D probes and two 1D probes. The last configuration [Fig. 4(c)] is a short wire with just two large 2D probes. We shall emphasize the short-wire limit ($L \ll l_\phi$) of Eq. (15) [given by Eq. (17)], since it is in this limit that the probes become important.

*Narrow-probes configuration.* First consider the case when all four probes have the same width as the wire itself, i.e., when $W_p = W$. In this case, $\eta = 2W/l_\phi = 2\alpha$. Putting this into Eq. (17), the equation appropriate for the short-wire limit, one finds that the amplitude of the weak-localization contribution in the short wire is exactly half that of the long wire [Eq. (17)]. This factor-of-2 reduction is due, of course, to the fact that there are two probes of width $W$ on either side of the wire. If instead of two, there were $N$ probes, then $\eta = N\alpha$, and we would expect a factor-of-$N$ reduction in the weak-localization contribution.

One can also reduce the amplitude of the localization contribution by increasing the width $W_p$ of the probes. For example, four probes of width $W_p = 2W$ would result in the same reduction as eight probes of width $W$. It would therefore seem difficult to distinguish experimentally these two cases. Applying a magnetic field, however, lets us distinguish between these two configurations. This can be seen by considering the characteristic field $B_c$ for the two configurations in the short-wire limit [Eq. (17)]. $B_c$ is defined as the half-width of the magnetoresistance curve; mathematically $(\Delta R/R)(B_c) = \frac{1}{2}(\Delta R/R)(0)$. For the former configuration (four probes of width $2W$ each), $B_c = [3\Phi_s/\pi 2Wl_\phi(0)]$, whereas for the latter it is exactly twice that. Thus, by simply looking at the total magnitude and the half-width of the weak localization MR in the short-wire limit, one can estimate both the number and the width of the 1D probes.

*1D wire with two 2D probes.* In this case $\eta_1 = 0$ and $\eta = \eta_2$. In general, the presence of 2D probes results in a larger reduction in the magnitude of the weak-localization contribution in comparison to 1D probes. This can be seen by estimating the value of $\eta_2$ for realistic material parameters. Let $\theta = \pi$, $l_{\phi 2D} = 1$ $\mu$m, and $l = 0.01$ $\mu$m, giving $\eta_2 = 0.59$. In comparison, $\eta$ for the narrow probes configuration, with $W_p = 0.1$ $\mu$m and $l_\phi = 1.0$ $\mu$m, is 0.2, so that the magnitude of the weak-localization contribution for a wire with two 2D probes is less than half that for the corresponding narrow-probes configuration in the short-wire limit.

Even more striking, however, is the magnetoresistance of this configuration in the short-wire limit. Putting $\eta_2$ defined by Eq. (19) (with $\theta = \pi$) into Eq. (17), we obtain

$$\frac{\Delta R}{R} = \frac{R_\square}{(\pi\hbar/e^2)}\frac{1}{\eta} = \frac{R_\square}{(2\pi^2\hbar/e^2)}\left[\psi\left[\frac{1}{2}+\frac{B_\phi}{B}\right]+\ln\left[\frac{B}{4B_0}\right]\right]. \quad (20)$$

This is identical in form to the theoretical weak-localization MR for a *macroscopic* 2D film.[15,16] To visually demonstrate the difference this causes in the MR, we show in Fig. 5 the experimental MR of two macroscopic Ag samples. The first [Fig. 5(a)] is a long ($\simeq 50$ $\mu$m) 1D wire, and the second [Fig. 5(b)] is a large 2D film. It can be seen in Fig. 5(b) that the MR changes very rapidly at very small magnetic fields: this is the characteristic signature of a 2D film, and we should expect to see this signature in short wires with 2D probes.

*Wide-probes configuration.* This is just the configuration which was used to derive Eq. (15), with $\eta = \eta_1 + \eta_2$, $\eta_1$ and $\eta_2$ being defined as before, in the paragraph preceding Eq. (14b). The combination of 1D and 2D probes makes the situation a bit complicated. Due to the presence of the 2D probes, the amplitude of the weak-localization contribution is less than that for the narrow-probes configuration. The magnetic-field dependence is also more complicated then either of the two configurations discussed above, being a combination of 1D and 2D MR. One should still expect to see the magnetic-field dependence of the 2D pads in the short-wire limit, although it will be less pronounced than for a wire with only 2D pads.

*Other geometries.* Quite frequently, experimental four-probe configurations are more complicated than the ex-

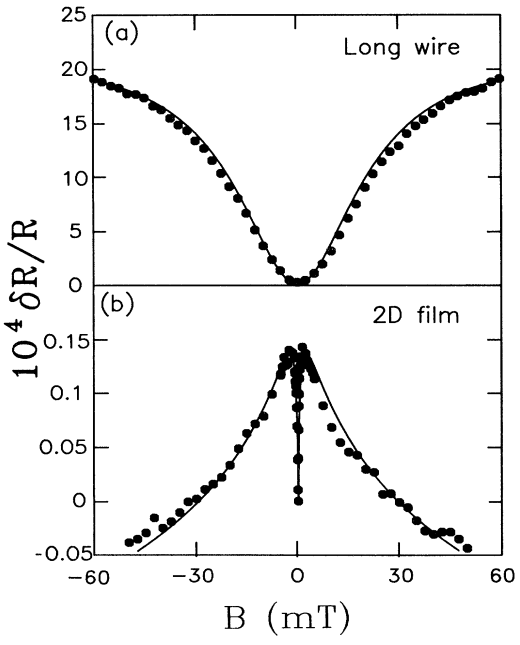


FIG. 5. Weak-localization magnetoresistance of a long one-dimensional Ag wire and two-dimensional Ag film at 2.0 K. Circles, data; solid lines, fits to weak localization theory. (a) $\sim 50$-$\mu$m-long wire, width 35 nm, fitting parameters $l_\phi = 1.9$ $\mu$m, $l_{so} = 0.39$ $\mu$m. $B_c \simeq 38$ mT. (b) Two-dimensional film, length 5 mm, width 50 $\mu$m, fitting parameters $l_\phi = 3.61$ $\mu$m, $l_{so} = 0.58$ $\mu$m. The sharp rise close to zero magnetic field corresponds to $B_c \simeq 0.5$ mT.

amples we have discussed. For example, a favorite configuration is one in which the widths of the probes rae increased in steps as one goes away from the 1D wire. To calculate the weak-localization contribution for such a sample would involve solving more than three-node equations. However, all such situations can be reduced to the three-node case, with a more complicated expression for the parameter $\eta$.

*Single Loops.* In the Introduction, we mentioned the problems associated with obtaining a full quantitative understanding of the $h/2e$ Aharonov-Bohm effect in some of the single metal loops studied at Yale University. These problems were associated with the effects of the measurement probes attached to the loops. Unfortunately, because of the complicated probe arrangement in these samples, which was dictated by considerations of lithography, these samples are difficult to model theoretically. Recently, Verbruggen *et al.*[24] have measured single micron-size Au loops with the sample geometry shown in the inset to Fig. 6. Using the formalism that we have developed, we can derive the weak-localization contribution for this geometry:

$$\frac{\Delta R}{R}=\frac{R_\square}{\pi\hbar/e^2}\frac{l_\phi}{W}\times\left[\frac{1+\delta^2+2\delta\coth 2b-(l_\phi/b)(\delta^2\tanh b+\delta)}{\delta^2\tanh b+2\delta+\coth 2b-(\cos\gamma/\sinh 2b)}\right], \tag{21}$$

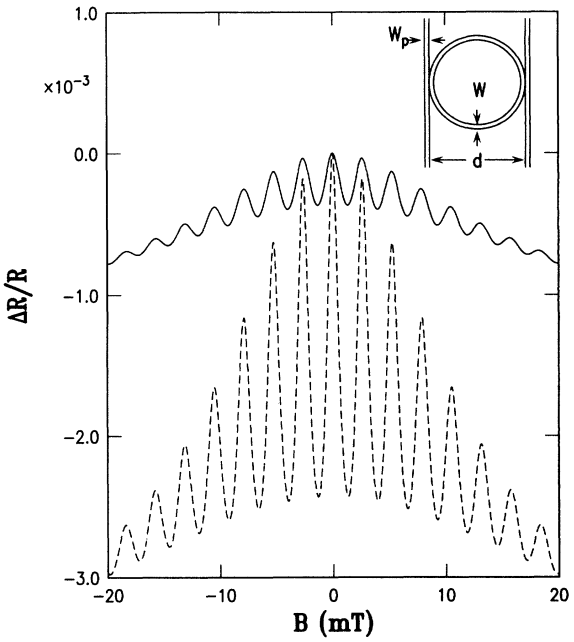


FIG. 6. Theoretical predictions for magnetoresistance of a single loop with probes in the configuration of Ref. 25 (see inset). Diameter of the loop $d=1$ $\mu$m, linewidth $W=50$ nm, and width of the probes $W_p=50$ nm. Dashed line is the AAS theory for an isolated loop and the solid line is the result of our calculations for $l_\phi=2$ $\mu$m.

where $\gamma=2\pi\Phi/\Phi_s$, where $\Phi$ is the flux through the loop, $\delta=\eta_1/\alpha$, $\eta_1=W_p/l_{\phi p}$, $\alpha=W/l_\phi$, the circumference of the loop is $2b$, the width of wire defining the loop is $W$, and the width of the probes is $W_p$. As before, the arguments of the hyperbolic function are all normalized to $l_\phi$.

Note that, as the circumference of the loop becomes large in comparison to $l_\phi$, we regain the result for a long wire, Eq. (16). As the width of the probes is reduced ($\delta\rightarrow 0$), we obtain the result of Altshuler, Aharonov, and Spivak for an isolated single loop. It is clear from Fig. 6 that the presence of probes suppresses the amplitude of the $h/2e$ Aharonov-Bohm oscillations substantially, in agreement with previous calculations.[25] We refer to Ref. 24 for a direct comparison between the theory and experiment. The results confirm the need to take the measurement probes into account to describe the experimental data.

#### 4. *Physical interpretation*

From the examples above, it is clear that the probes affect both the *magnitude* and the *shape* of the weak-localization MR. This effect of the measurement probes on the MR can be explained very simply using the well-known physical picture of weak localization introduced by Khmelnitskii[26] and Bergmann.[15] For a mesoscopic wire, the weak-localization correction includes contributions from time-reversed paths which originate in the wire, but then diffuse into the probes. In the short-wire limit ($L\ll l_\phi$), the interfering electrons spend most of their time in probes. The wider the 1D probe, the smaller the probability that the electrons will return to the origin in the wire phase coherently; the probability is smallest for a wire with 2D probes. Thus the magnitude of the weak-localization contribution is smaller for wires with wider probes. The effect of the probes on the shape of the MR can be understood in a similar way. For a wire with 1D probes, the area of the interfering paths is restricted by the width of the probes. The larger the width, the smaller the magnetic field required to suppress the weak-localization contribution, and consequently, the smaller the characteristic field $B_c$ of the MR. For a wire with 2D probes, however, the area of these paths is restricted only by $l_\phi$. As in the case of a 2D film, where $B_c\simeq\Phi_s/l_\phi^2$, a small magnetic field will rapidly suppress the contribution of these paths, and we should expect the MR of such a wire to resemble the MR of a 2D film (Fig. 5).

Two-dimensional probes have the most visible effect on the MR of a short wire: because of the large value of $\eta$, the magnitude of the MR is greatly reduced, and the characteristic magnetic-field dependence of the 2D probes contrasts with the MR signature of the 1D wire. One-dimensional probes also affect the magnitude and the shape of the MR, but the effects are less dramatic. The effect of 1D probes on the shape of the MR is greatest when they are of a different width than the 1D wire. However, ignoring the effects of 1D probes, even narrow ones, can lead to errors in the quantitative analysis of the MR data of short wires.

### B. Conductance fluctuations

#### 1. General formulation

Much of the formalism that we have developed for calculating the weak-localization contribution of small multiprobe 1D wires can also be used to calculate the amplitude of the conductance fluctuations in these geometries. Although the detailed physical interpretation of the conductance fluctuations in terms of interfering electrons is less direct, mathematically the technique is relatively straightforward. We restrict ourselves to the low-temperature limit, where $l_T \equiv \sqrt{\hbar D/k_B T} \gg l_\phi$. Realistically, very few metallic samples fall in this regime, unless $l_\phi$ saturates at low temperatures (e.g., due to the presence of paramagnetic impurities at low magnetic fields). Even in the case of samples prepared from silicon or gallium arsenide, $l_T$ is rarely more than a few times $l_\phi$. Nonetheless, we expect the qualitative effects that the probes have on conductance fluctuations in the low-temperature regime to be the same as in the high-temperature regime.

Conforming to the literature on fluctuations in multiprobe samples, we shall discuss fluctuations in the voltage $V_{ab,cd}$ rather than fluctuations in the conductance. Our starting point is Eq. (4), generalized to a nonzero magnetic field $B$,

$$\Delta V_{ab,cd}(B) = -\frac{1}{\sigma_0^2}\int_a^b \frac{dr}{S(r)} \int dS(r) \int_c^d d^3r' \Delta\sigma(r,r',B) \times \langle j^{\rm cl}(r') \rangle , \tag{22}$$

where $\langle j^{\rm cl}(r') \rangle = \langle E^{\rm cl}(r') \rangle / \sigma_0$ is the classical current density. We wish to calculate the correlation function of $\Delta V_{ab,cd}$, defined by

$$F(\Delta B) = \langle \Delta V_{ab,cd}(B) \Delta V_{ab,cd}(B+\Delta B) \rangle , \tag{23}$$

where the angular brackets denote an average over the magnetic field $B$. According to the ergodic hypothesis of Altshuler[5] and Lee and Stone,[6] this is equivalent to an average over all possible impurity configurations. Following the notation of Benoit *et al.*,[7] we decompose $F(\Delta B)$ into components that are symmetric and antisymmetric with respect to the magnetic field

$$F^S(\Delta B) = \langle \Delta V^S_{ab,cd}(B) \Delta V^S_{ab,cd}(B+\Delta B) \rangle \tag{24a}$$

and

$$F^A(\Delta B) = \langle \Delta V^A_{ab,cd}(B) \Delta V^A_{ab,cd}(B+\Delta B) \rangle , \tag{24b}$$

where

$$\Delta V^{S,A}_{ab,cd}(B) = [\Delta V_{ab,cd}(B) \pm \Delta V_{ab,cd}(-B)]/2 . \tag{25}$$

With $\Delta\sigma(r_1,r_2)\Delta\sigma(r_3,r_4) = |d(r_1,r_2)|^2 \delta(\mathbf{r}_1-\mathbf{r}_3)\delta(\mathbf{r}_2-\mathbf{r}_4)$ and using the Onsager relation $\Delta\sigma(r,r',B) = \Delta\sigma(r',r,-B)$, one obtains[10]

$$F^S(\Delta B) = 2\left[\frac{e^2 D}{\pi\sigma_0^2}\right] \int_a^b \frac{dr_1}{S(r_1)} \int dS(r_1) \int_c^d d^3r_2 \int_a^b \frac{dr_3}{S(r_3)} \int dS(r_3) \int_c^d d^3r_4 |d(r_1,r_2,\Delta B)|^2 \times [\delta(\mathbf{r}_1-\mathbf{r}_3)\delta(\mathbf{r}_2-\mathbf{r}_4) + \delta(\mathbf{r}_1-\mathbf{r}_4)\delta(\mathbf{r}_2-\mathbf{r}_3)] \times j^{\rm cl}(\mathbf{r}_2) j^{\rm cl}(\mathbf{r}_4) , \tag{26a}$$

$$F^A(\Delta B) = 2\left[\frac{e^2 D}{\pi\sigma_0^2}\right] \int_a^b \frac{dr_1}{S(r_1)} \int dS(r_1) \int_c^d d^3r_2 \int_a^b \frac{dr_3}{S(r_3)} \int dS(r_3) \int_c^d d^3r_4 |d(r_1,r_2,\Delta B)|^2 \times [\delta(\mathbf{r}_1-\mathbf{r}_3)\delta(\mathbf{r}_2-\mathbf{r}_4) - \delta(\mathbf{r}_1-\mathbf{r}_4)\delta(\mathbf{r}_2-\mathbf{r}_3)] \times j^{\rm cl}(\mathbf{r}_2) j^{\rm cl}(\mathbf{r}_4) , \tag{26b}$$

where the particle-hole propagator $d(\mathbf{r}_1,\mathbf{r}_2,\Delta B)$ is the solution of the diffusion equation

$$\left[\left(-i\nabla - \frac{e\Delta\mathbf{A}}{\hbar}\right)^2 + \frac{1}{l_\phi^2}\right] d(\mathbf{r},\mathbf{r}') = \frac{\delta(\mathbf{r}-\mathbf{r}')}{\hbar D} . \tag{27}$$

This equation is identical to Eq. (6) for $C(\mathbf{r},\mathbf{r}')$, with $\mathbf{A}$ replaced by $\Delta\mathbf{A}/2$. $F(\Delta B)$ given above does not include the particle-particle channel contribution, which is equal to the particle-hole contribution at zero field, but is rapidly suppressed at magnetic fields larger than $\sim B_c$. Thus our results will only be valid at high magnetic fields.

In our discussion above, we have assumed that $l_\phi$ in Eq. (27) is the same as the phase coherence length applicable to the weak-localization case, Eq. (6). There are reasons to expect that this may not be the case. In the Feynman diagrams[2] for conductance fluctuations, one does not allow inelastic processes to connect the two conductivity loops. This means that the amplitude of the conductance fluctuations is determined by the quasiparticle scattering time due to electron-electron interactions, while weak localization is determined by the lifetime of the Cooper channel.[22] For the moment, we shall ignore this difference, with the understanding that $l_\phi$ refers to the appropriate phase coherence length.

We shall now apply these formulas to the calculation of the correlation function for a wire with the geometry shown in Fig. 2. As before, we assume that the current is introduced through two probes $c$ and $d$ and that the voltage is measured across the two other probes $a$ and $b$. The region common to both the path between the current probes and the path between the voltage probes we shall denote by $s$.

Due to the $\delta$ functions in Eq. (26), the regions of integration over the coordinates $r_1$, $r_2$, $r_3$, and $r_4$ are restricted. We can define a function $F^{SA}(\Delta B)=F^{S}(\Delta B)-F^{A}(\Delta B)$, the contributions to which come only from the part of the sample common to both the current and the voltage paths. From Eq. (26), this is given by

$$F^{SA}(\Delta B)=2\left[\frac{e^2D}{\pi\sigma_0^2}\right]\int_{r_1\in s}\frac{dr_1}{S(r_1)}\int dS(r_1)\int_{r_2\in s}d^3r_2|d(r_1,r_2,\Delta B)|^2[j^{\rm cl}(r_2)]^2\ , \tag{28a}$$

where the notations $r_1\in s$ and $r_2\in s$ imply that the region of integration is in the region of the sample common to both the voltage and the current paths. The contributions to $F^{A}(\Delta B)$ come from the remaining regions of integration

$$F^{A}(\Delta B)=2\left[\frac{e^2D}{\pi\sigma_0^2}\right]\int_{r_1\in a,b,s}\frac{dr_1}{S(r_1)}\int dS(r_1)\int_{r_2\in c,d,s}d^3r_2|d(r_1,r_2,\Delta B)|^2[j^{\rm cl}(r_2)]^2\ , \tag{28b}$$

where it is understood that $r_1$ and $r_2$ are not both simultaneously in the region $s$. To evaluate these integrals, we first need to solve the diffusion equation [Eq. (27)] to determine $d(r,r')$. This we solve using the same technique we employed for the weak-localization problem; the difference is that $r$ and $r'$ are no longer restricted to be in the sample region $s$, but can now also be in the probe regions $a$, $b$, $c$, and $d$.

$F^{A}(\Delta B)$, involving as it does integrals over the probes, is intimately dependent on the nature of the probes, and to calculate it we need to consider specific probe configurations. $F^{SA}(\Delta B)$, on the other hand, like the weak-localization contribution, only involves integrals over the region $s$. We can carry out the integral in Eq. (28a) for any probe configuration to obtain

$$F^{SA}=2\left[\frac{e^2I}{h\sigma_0^2t^2}\right]^2\frac{Ll_\phi^3}{W^4}\left[\frac{(\eta^2+\alpha^2)\coth L-(l_\phi/L)(\eta^2-\alpha^2)+2\alpha\eta}{\eta^2+\alpha^2+2\alpha\eta\coth L}\right.$$
$$\left.-2\alpha\eta\frac{l_\phi}{L}\left[\frac{2\alpha\eta+(\eta^2+\alpha^2)\coth L}{[(\eta^2+\alpha^2)+2\alpha\eta\coth L]^2}\right]+\frac{(\eta^2-\alpha^2)^2(L/l_\phi)+2\alpha\eta(\eta^2-\alpha^2)}{[(\eta^2+\alpha^2)\sinh L+2\alpha\eta\cosh L]^2}\right]\ . \tag{29}$$

Again, this equation is valid for *any* probe configuration; different probe configurations correspond to different values of $\eta$. To determine $F^{A}$ and $F^{S}$, we need to take a look at specific probe configurations. As examples, we shall examine two: the narrow-probes configuration [Fig. 4(a)] and the wide-probes configuration {Fig. 4(b)].

### 2. *Narrow-probes configuration*

Let us now consider the case of a wire where all the probes are of equal width $W_p\ll l_\phi$. The contributions to $F^{A}(\Delta B)$ can be split into components which we label *ac*, *ad*, *as*, *bc*, *bd*, *bs*, *sc*, and *sd*, referring to Fig. 4(a). The first letter corresponds to the region of integration over $r_1$ and the second letter refers to the region of integration over $r_2$. By symmetry it can be seen that $ac=bd$, $ad=bc$, $bs=as$, $sd=sc$, and $sc=as$. Thus we need to evaluate only the three contributions: *ac*, *as*, and *ad*. The total contribution is equal to $2ac+2ad+4as$. Recalling that $\langle j^{\rm cl}(r_2)\rangle=I/tW_p$ for the 1D probes, we obtain (after tedious algebra)

$$F^{A}(\Delta B)=2\left[\frac{e^2I}{h\sigma_0^2t^2}\right]^2\left[\frac{(\eta^2+\alpha^2)\cosh 2L-(\eta^2-3\alpha^2)+2\alpha\eta\sinh 2L}{\eta^2[(\eta^2+\alpha^2)\sinh L+2\alpha\eta\cosh L]^2}\right.$$
$$\left.+2\frac{[(\eta^2+\alpha^2)\sinh 2L-(2L/l_\phi)(\eta^2-\alpha^2)+2\alpha\eta(\cosh 2L-1)]}{\alpha\eta[(\eta^2+\alpha^2)\sinh L+2\alpha\eta\cosh L]^2}\right]\ . \tag{30}$$

Here $\alpha=W/l_\phi$, $\eta=2W_p/l_{\phi p}$, and the arguments of the hyperbolic functions are normalized by $l_\phi$.

*Length dependence.* Equations (29) and (30) appear quite complicated, but have some very simple limits. For long wires ($L\gg l_\phi$), they reduce to

$$F^{S}\simeq F^{A}(0)+2\left[\frac{e^2I}{h\sigma_0^2t^2}\right]^2\frac{L}{W}\frac{1}{\alpha^3} \tag{31a}$$

and

$$F^{A}(0)\simeq 2\left[\frac{e^2I}{h\sigma_0^2t^2}\right]^2\left[\frac{1}{\eta}+\frac{2}{\alpha}\right]\frac{1}{\eta(\eta+\alpha)^2}\ . \tag{31b}$$

Note that the second term in Eq. (31a) for $F^{S}(\Delta B)$, which is the dominant term for $L\gg l_\phi$, is independent of any parameter related to the measurement probes, as expect-

ed. In terms of fluctuations in the conductance $G$, this term gives $(\Delta G)\sim(l_\phi/L)^{3/2}$, the value predicted by the two-probe theories of Altshuler[5] and Lee and Stone.[6] The antisymmetric contribution $F^A$, however, is still dependent on the probes, through $\eta$.

For short wires ($L \ll l_\phi$), Eqs. (29) and (30) give

$$F^S, F^A \rightarrow 2\left[\frac{e^2 I}{h\sigma_0^2 t^2}\right]^2 \frac{1}{\eta^4} . \tag{32}$$

As we saw in the case of localization, the voltage fluctuations in this limit depend only on parameters related to the probes. Large values of $\eta$ due to large probes result in smaller fluctuations. The amplitude of the voltage fluctuations has a stronger dependence on the size of the probes than the weak-localization MR, decreasing as $\eta^{-2}$ rather than $\eta^{-1}$ [see Eq. (17)].

Figure 7 shows a plot of the symmetric and antisymmetric voltage fluctuations obtained from Eqs. (29) and (30) as a function of the length $L$ of the sample, for the case $W_p = W$. Conforming to the literature, we plot $(\Delta V/\Delta V_\phi) = \sqrt{F}/\Delta V_\phi$, where the normalization factor $\Delta V_\phi$, introduced by Benoit *et al.*,[3] is defined as $\Delta V_\phi = I(e^2/\hbar) l_\phi^2/\sigma_0^2 t^2 W^2$. The antisymmetric voltage fluctuations are seen to be essentially independent of the length of the sample. The symmetric fluctuations scale as $(L/l_\phi)^{1/2}$ for $L \gg l_\phi$, corresponding to a scaling law for conductance fluctuations of $(\Delta G)\sim(l_\phi/L)^{3/2}$, as expected from the two-probe theories. In the opposite limit ($L \ll l_\phi$), the symmetric voltage fluctuations have the same asymptotic value as the antisymmetric voltage fluctuations. Similar theoretical results have been obtained previously by various authors[10,13,14] and agree qualitatively with the experiments of Benoit *et al.*[3] and Skocpol *et al.*[4]

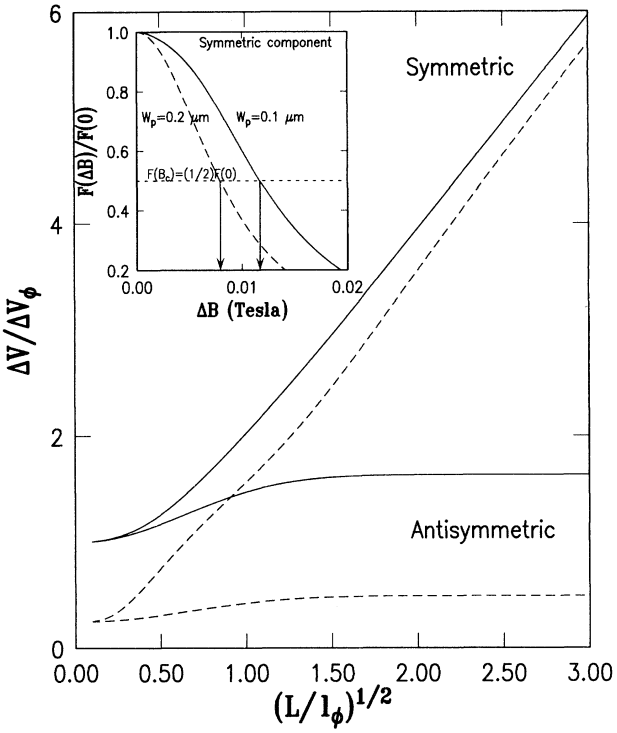


FIG. 7. Theoretical predictions for the zero-magnetic-field symmetric and antisymmetric voltage fluctuations of short wires of length $L$ and width $W$, with different probe configurations, as a function of $L$ normalized to $l_\phi$. $l_\phi = 2.0$ $\mu$m and $W = 0.1$ $\mu$m. Solid line, short wire with four one-dimensional probes of width $W_p = W$; dashed line, short wire with four one-dimensional probes of width $W_p = 2W$. Inset: field correlation function of the symmetric component of the voltage fluctuations for a short wire with four one-dimensional probes, with $L = 1.0$ $\mu$m, $l_\phi = 2.0$ $\mu$m, and $W = 0.1$ $\mu$m. Solid line, $W_p = W$; dashed line, $W_p = 2W$. The arrows mark the value of the correlation field $B_c$ for each of the two curves.

For comparison, we also show in the same figure the voltage fluctuations for a wire with probes of width $W_p = 2W$. The functional dependence on the length is quite similar, but the amplitude of the fluctuations is reduced, as expected from the analysis presented above.

*Nonlocal case.* Unlike weak localization, one can obtain a contribution to the voltage fluctuations even from the parts of the sample through which there flows no classical current. For example, suppose we introduce the current through $c$ and $a$ and measure voltage between $b$ and $d$ [Fig. 4(a)]. Since there is no region common to both the current and voltage paths, $F^{SA}$ is zero and hence $F^S = F^A$. The only contributions to the voltage fluctuations come from the terms $ba$, $bc$, $da$, and $dc$, all of which are equal for probes with equal width $W_p$. Thus

$$F^A = F^S = 32\left[\frac{e^2 I}{h\sigma_0^2 t^2}\right]^2 \times \left[\frac{\alpha^2}{\eta^2[(\eta^2+\alpha^2)\sinh L + 2\alpha\eta\cosh L]^2}\right] . \tag{33}$$

For long wires, $F^A(\Delta B)$ and $F^S(\Delta B)$ decrease exponentially with $L/l_\phi$.

*Magnetic-field dependence.* In our discussion of weak localization, we saw that the measurement probes affected both the magnitude and shape of the weak-localization magnetoresistance. For the fluctuations the quantity analogous to the weak-localization MR is the autocorrelation function $F(\Delta B)$, defined by Eq. (23). For the narrow-probes configuration, which has only 1D elements, the field dependence[27] of $F(\Delta B)$ comes through the field dependence of $l_\phi$

$$\frac{1}{l_\phi^2(\Delta B)} = \frac{1}{l_\phi^2} + \frac{1}{3}\left[\frac{\pi W \Delta B}{\Phi_0}\right]^2 , \tag{34}$$

where $\Phi_0 = h/e$ is now the normal electron flux quantum. (A similar equation holds for $l_{\phi p}$, with $W$ replaced by $W_p$.) This is the same equation as Eq. (18) for weak localization, except that $B$ is replaced by $\Delta B/2$. Just as for weak localization, the characteristic field scale $B_c$, which is defined as the half-width of the autocorrelation func-

tion $F(B_c)=\frac{1}{2}F(0)$, is determined by $W$ and $W_p$. In the long-wire limit, $B_c$ is determined by the parameters $W$ and $l_\phi$ of the 1D wire itself, while in the short-wire limit, only the parameters $W_p$ and $l_{\phi p}$ of the probes are important. In the intermediate regime, $B_c$ depends on both $W$ and $W_p$ in a nontrivial way. This means that when $W \neq W_p$ one should expect to see a change in $B_c$ as one goes from a long wire to a short wire. In addition, in the short-wire limit, wires with probes of different widths will have different characteristic fields even though the width of the wire is the same. This is demonstrated in the inset to Fig. 7, which shows a plot of $F^S(\Delta B)$ for the two cases $W_p = W$ and $2W$, with $L = \frac{1}{2}l_\phi$.

More surprising, however, is the fact that $B_c$ is a function of the length of the sample even for wires with probes of the same width as the wire. Figure 8 shows a plot of $B_c$ as a function of $[L/l_\phi(0)]$ for a wire in the narrow-probes configuration, with $W_p = W$. On the positive abscissa, we have plotted the results for the local case, i.e., the case when the current is introduced through the probes $c$ and $d$, and the voltage measured across probes $a$ and $b$. On the negative abscissa, we have plotted results for the nonlocal case. In the local case, for large $[L/l_\phi(0)]$, $B_c$ approaches the value 0.42 $[\phi_0/l_\phi(0)W]$ predicted by the two-probe theory.[27] As $[L/l_\phi(0)] \to 0$, however, $B_c$ decreases, and continues to decrease as we cross over into the nonlocal regime.

This implies that one cannot accurately determine $l_\phi(0)$ in the mesoscopic size regime from $B_c$ by using a simple relation of the form $B_c = \text{constant} \times [\Phi_0/l_\phi(0)W]$. The application of such a relation in the region $L \sim \frac{1}{2}l_\phi$, for example, would give an erroneously large value of $l_\phi(0)$. To determine $l_\phi(0)$ one must fit $F(\Delta B)$ as a function of $\Delta B$, with $l_\phi$ as a fitting parameter, much as one fits the low-field magnetoresistance in the case of weak localization.

It is worth noting that, at low magnetic fields, $B_c$ depends on the absolute magnetic field $B$. This is due to the magnetic-field dependence of the contribution[2] from the particle-particle (Cooper) channel to $F(\Delta B)$. $B_c$ for the particle-hole contribution (diffusion channel) does not depend on $B$. For $B = 0$, the contributions from both channels are equal and consequently, $B_c$ is just that of the diffusion channel. At large magnetic fields

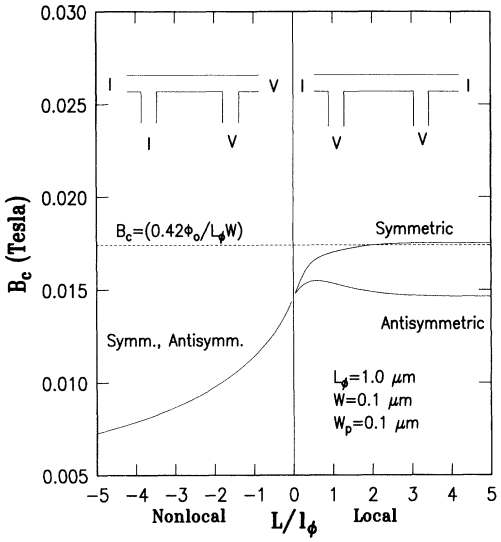


FIG. 8. $B_c$ of the symmetric and antisymmetric conductance-conductance correlation functions for a short wire of width $W = 0.1$ μm with four one-dimensional probes of width $W_p = W$ and $l_\phi = 1.0$ μm, as a function of the length of the sample. Positive abscissa, local case; negative abscissa, nonlocal case. Current and voltage contacts for each case are shown in the insets. Dashed line shows the value of $B_c$ predicted by the two-probe theory.

$(B > \Phi_s/Wl_\phi)$, the Cooper channel is suppressed, so that $B_c$ is again that of the diffusion channel. For intermediate values of $B$, both channels contribute. $B_c$ for the Cooper channel will increase due to the relevant field dependence of $l_\phi$ given by Eq. (18) since $B_c \propto 1/l_\phi(B + \Delta B/2)$. Thus for these intermediate values of $B$ there will be an increase in $B_c$ over the zero field $(B = 0)$ value; but this increase will be small due to the overall suppression of the Cooper channel contribution.

### 3. *Wide-probes configuration*

Finally we discuss the case of a wire with two narrow voltage probes and two 2D probes. $F^A(\Delta B)$ is given by

$$F^A(\Delta B) = \left[\frac{e^2 I}{h\sigma_0^2 t^2}\right]^2 \left\{4\left[\frac{\mathcal{J}}{\theta}\right]\left[\Gamma\left[\frac{1}{2}+\frac{2B_\phi}{\Delta B}\right]\right]^2\left[\psi\left[\frac{1}{2}+\frac{2B_\phi}{\Delta B}\right]+\ln\left[\frac{B}{8B_0}\right]\right]^{-2}\right.$$
$$\times\left[\frac{(\eta^2+\alpha^2)\cosh 2L-(\eta^2-3\alpha^2)+2\alpha\eta\sinh 2L}{\eta[(\eta^2+\alpha^2)\sinh 2L+2\alpha\eta\cosh 2L]^2}\right.$$
$$\left.+\frac{(\eta^2+\alpha^2)\sinh 2L-(2L/l_\phi)(\eta^2-\alpha^2)+2\alpha\eta(\cosh 2L-1)}{\alpha[(\eta^2+\alpha^2)\sinh L+2\alpha\eta\cosh L]^2}\right]$$
$$\left.+2\left[\frac{(\eta^2+\alpha^2)\sinh 2L-(2L/l_\phi)(\eta^2-\alpha^2)+2\alpha\eta(\cosh 2L-1)}{\alpha\eta[(\eta^2+\alpha^2)\sinh L+2\alpha\eta\cosh L]^2}\right]\right\}. \quad (35)$$

Here $\theta$ is the angle subtended by each of the 2D probes at either end of the wire. $\mathcal{J}$ is the integral

$$\mathcal{J}=\int_l^\infty \frac{dr}{r}\exp\left[-\left[\frac{\pi\Delta B r^2}{\Phi_0}\right]\right] \times\Psi^2\left[\frac{1}{2}+\frac{2B_\phi}{\Delta B},1;\left[\frac{\pi\Delta B}{\Phi_0}\right]r^2\right], \quad (36)$$

where $\Psi$ is the confluent hypergeometric function of the second kind. Unfortunately, it is not possible to evaluate $\mathcal{J}$ in closed form for all values of $\Delta B$. We can approximate it for small values of $B$ by replacing the upper limit by $2l_\phi$. We then have

$$\mathcal{J}=\left[\frac{\left[\psi\left[\frac{1}{2}+\frac{2B_\phi}{\Delta B}\right]+\ln\left[\frac{\Delta B}{8B_0}\right]\right]^2}{\left[\Gamma\left[\frac{1}{2}+\frac{2B_\phi}{\Delta B}\right]\right]^2}\right]\ln(2l_\phi/l) . \quad (37)$$

Equations (35) and (36) are far too complicated for us to evaluate anything but the simplest limits without resorting to a computer. In zero field, the amplitude of both the symmetric and the antisymmetric voltage fluctuations are smaller than those obtained for the wire with four narrow probes, as shown in Fig. 7. With regard to the field dependence, we have found that, due to the complexity of the integral $\mathcal{J}$, the field dependence of $F(\Delta B)$ in this configuration is difficult to calculate, even numerically. However, due to the presence of the logarithmic terms in Eqs. (35) and (36), we expect to see a cusp in the correlation function at zero field, similar to the cusp seen in the weak-localization MR of wires in the wide-probes configuration.

## III. COMPARISON WITH EXPERIMENT

The existence of quantum-interference effects in mesoscopic samples has been demonstrated in many experimental systems, and it is not our intention to present an elaborate review here. Instead, we will concentrate on those studies where our insight into the effects of measurement probes could prove useful.

Although weak localization has been the most extensively studied quantum-interference effect, the importance of measurement probes came to be recognized only after the experiments of Benoit *et al.*[3] and Skocpol *et al.*[4] on conductance fluctuations in small metal and semiconductor wires. Consequently, we shall begin with a discussion of these experiments on fluctuations in small metallic systems. We shall then discuss some early work on weak localization in short metal wires, pointing out how the anomalous results of these experiments (which were not fully understood at the time) can be explained if one takes into account the effects of measurement probes. Finally, we shall discuss the results of a set of experiments we performed to demonstrate the effects of probes on quantum interference in mesoscopic Ag wires with different probe configurations.

### A. Conductance fluctuations

Benoit *et al.*[3] reported the results of a detailed study of conductance fluctuations in Au and Sb wires. These devices had multiple measurement probes, so that the fluctuations could be measured simultaneously in wires of different lengths. This work demonstrated that the amplitude of the fluctuations could be considered "universal" only on the scale of $l_\phi$: for wires with measurement probes closer than $l_\phi$, the authors observed conductance fluctuations of amplitude much larger than $e^2/h$. Similar results were also obtained by Skocpol *et al.*[4]

Benoit *et al.* also showed that a description in terms of voltage (or, equivalently, resistance) fluctuations appeared to be more fundamental than a description in terms of fluctuations in the conductance of a sample. They found that for very small samples, the fluctuations in the voltage across the sample were essentially independent of the length of the sample. Their results are reproduced in Fig. 9, which shows the symmetric and antisymmetric (with respect to magnetic field) voltage fluctuations as a function of the length of the sample normalized to $l_\phi$. The antisymmetric voltage fluctuations are essentially independent of the length of the sample. For $L<l_\phi$, the symmetric voltage fluctuations are also independent of the length of the sample; for $L>l_\phi$, however, they grow as $(L/l_\phi)^{1/2}$, consistent with the predictions of the two probe theories. We have also plotted in Fig. 9 the theoretical predictions of Eqs. (29) and (30), multiplied by a constant to agree with the data in the limit $L\to 0$. In spite of the fact that the data are for samples

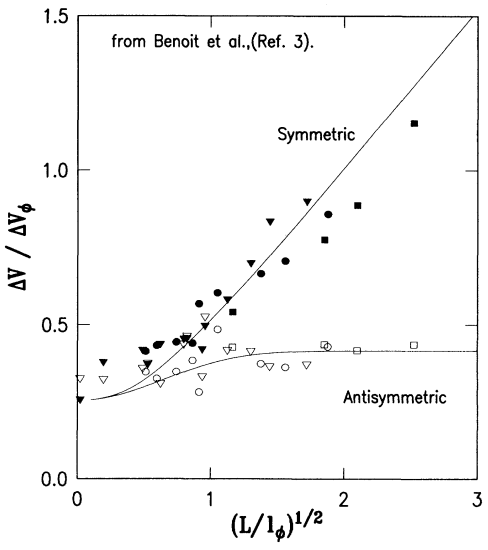


FIG. 9. Experimental symmetric and antisymmetric voltage fluctuations of one-dimensional Au and Sb metal wires, from Ref. 3. Solid symbols, symmetric contributions; open symbols, antisymmetric contributions. Circles, Sb sample at 40 mK; triangles, Sb sample at 300 mK; squares, Au sample at 40 mK. Solid curves, theoretical predictions of Eqs. (29) and (30), multiplied by a constant to agree with the data in the limit $L\to 0$.

with multiple measurement probes, and the theory describes samples with only four measurement probes, the agreement is still quite encouraging.

More recently, Haucke *et al.*[28] have reported measurements of the correlation field $B_c$ for these same Au and Sb wires. Their results are reproduced in Fig. 10, for both the local and the nonlocal case. The similarity to the theoretical predictions shown in Fig. 8 is evident. Once again, this emphasizes the fact that the correlation field is strongly dependent on the probes, and that, in the mesoscopic size regime, one cannot use $B_c$ alone to determine the phase coherence length.

Thus, as predicted, measurement probes affect both the magnitude and the magnetic-field dependence of the fluctuations in mesoscopic samples. It should be pointed, however, that the presence of intermediate spin-orbit scattering will also affect the amplitude and characteristic field scale of the fluctuations.[29] The difference between the effect of spin-orbit scattering and that of probes is that the effects of spin-orbit scattering can be seen even in macroscopic samples. For the proper analysis of data from mesoscopic samples, one should include the effects of measurements probes as well as spin-orbit scattering.

### B. Weak localization

#### *Narrow wires*

One of the first experiments on short 1D wires was performed by Masden and Giordano.[30] They measured the resistance of AuPd wires of length $L = 0.2-1.0$ $\mu$m as a function of temperature. The wires connected two large Ag probes, as in the geometry of Fig. 4(c). The low-temperature resistance of such wires is expected to rise as the temperature is lowered due to contributions from weak-localization and electron-electron interaction effects. The authors observed such a resistance increase, but found that the magnitude of the resistance rise was dependent on the length of the wire, being smaller for the shorter samples. They interpreted their results as implying that the length of the sample acted as a cutoff for $l_\phi$. Since the 1D weak-localization contribution is proportional to $l_\phi$, this would imply a smaller contribution for the shorter wires. However, due to a lack of magnetoresistance data, they were not able to isolate the weak-localization contribution from the contribution of electron-electron interactions. In our way of thinking, the suppression of the weak-localization contribution for the shorter wires is due to the influence of the thick 2D probes, which reduce the amplitude of the interference when $L \simeq l_\phi$. Masden and Giordano's results are consistent with this picture. Similar results were obtained by Choi, Tsui, and Palmateer[31] in GaAs/$Al_xGa_{1-x}$As heterostructures.

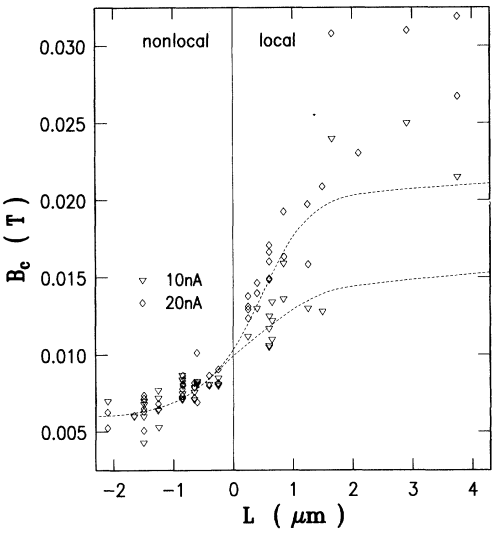


FIG. 10. Experimental correlation field $B_c$ of one-dimensional Au and Sb metal wires for local and nonlocal measurement configurations as a function of the length of the wires, from Haucke *et al.*, Ref. 28. Positive abscissa, local measurement; negative abscissa, nonlocal measurement. Triangles refer to data taken at 10-nA drive current; diamonds to data at 20-nA drive current. Dashed lines are guides to the eye.

Bishop and Dolan[32] measured weak localization in long Li wires doped heavily at regular intervals $L$ with Fe impurities. Since the magnetic Fe impurities should completely destroy phase coherence in the doped regions, their sample essentially consisted of a series of short wires, each of length $L$. The authors measured wires with different values of $L$, and found that the size of the weak-localization correction was proportional to $L$. Similar to Masden and Giordano, they also interpreted their results in terms of a length-dependent cutoff to $l_\phi$. Although the saturation observed was not related directly to the effect of measurement probes, their results can be described quite well by Eq. (15), with $\eta = \infty$. This value of $\eta$ corresponds to the boundary condition $C(r,r') = 0$ at the ends of each segment of length $L$, a boundary condition induced by the complete randomization caused by the Fe impurities at each doped region.

### C. Effects of probes on short silver wires

We now discuss the results of an experiment we performed to study the effect of measurement probe geometry on short silver wires. Some of the results of this study have already been published,[19] so we shall not discuss here the details of sample fabrication and measurement. The samples were fabricated in the two-measurement probe configurations shown in Figs. 4(a) and 4(b). Corresponding to each probe configuration, wires of two different lengths were studied, $\simeq 1.3$ and $\simeq 5$ $\mu$m. Long ($\simeq 50$ $\mu$m) wires and 2D films were codeposited along with the short wires for comparison of material parameters. Table I lists the relevant parameters of the short wires we measured.

Silver exhibits strong spin-orbit scattering; in the presence of such spin-dependent scattering, it is well known that the weak-localization contribution[15,16] breaks up into a singlet part and a triplet part

TABLE I. Sample parameters. $R_\square$ is at 4.5 K. Narrow-probe configuration corresponds to Fig. 4(a), wide probe configuration to Fig. 4(b). Values of $l_\phi$ are at 1.25 K, except for sample $B$, for which satisfactory fit at 1.25 K was not possible because of the presence of conductance fluctuations. $l_{so}$ for a particular sample was found to be independent of temperature (Ref. 22). Samples $A$, $B$, $C$, and $E$ were codeposited; samples $D$ and $F$ were codeposited.

| Sample | $R_\square$ ($\Omega$) | $L$ ($\mu$m) | Probe configuration | $l_\phi$(1.25 K) ($\mu$ m) | $l_{so}$ ($\mu$ m) |
|---|---|---|---|---|---|
| $A$ | 1.4 | 1.3 | Narrow | 2.2 | 0.43 |
| $B$ | 1.4 | 1.4 | Wide | 1.3 (3.5 K) | 0.41 |
| $C$ | 2.2 | 4.9 | Narrow | 1.5 | 0.30 |
| $D$ | 1.1 | 4.8 | Wide | 3.0 | 0.65 |
| $E$ | 1.4 | 53 | Long wire | 2.3 | 0.39 |
| $F$ | 1.2 | 53 | Long wire | 2.9 | 0.51 |

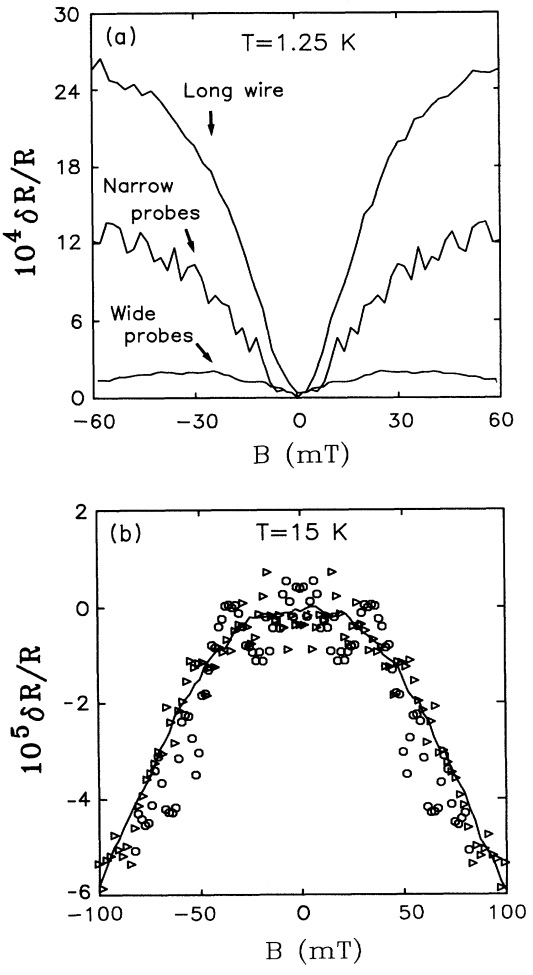


FIG. 11. (a) Symmetric component of the experimental magnetoresistance of $L\sim1.3$-$\mu$m Ag wires, samples $A$ and $B$, along with their codeposited long wire, sample $E$, 1.25 K. Sample $A$ is a short wire in the narrow-probes configuration [$W_p=W$, Fig. 4(a)]; sample $B$ is in the wide-probes configuration [Fig. 4(b)]. $l_\phi$ as determined by weak-localization fits to the data from the long wire is 2.39 $\mu$m. (b) Data for the same three wires at 15 K. Solid line, long wire, sample $E$; triangles, sample $A$; circles, sample $B$. $l_\phi$ at this temperature is 0.29 $\mu$m.

$$\frac{\Delta R}{R}=-\tfrac{3}{2}f(l_2)+\tfrac{1}{2}f(l_\phi)\ , \tag{38}$$

where $f(l_\phi)$ is the magnetoresistance formula appropriate to the sample geometry, and $l_2$ is given by

$$l_2^{-2}=l_\phi^{-2}+\tfrac{4}{3}l_{so}^{-2}\ . \tag{39}$$

This leads to a positive MR at low magnetic fields instead of the negative MR expected from Eq. (15).

The magnetoresistance of our short wires is in general asymmetric with respect to the zero of magnetic field due to the presence of sample specific effects. Such asymmetries have been seen in short metal wires by many groups.[1] For weak localization, we are only interested in the symmetric contribution, since the weak localization is expected to be symmetric. Thus all the weak-localization MR shown below has been symmetrized with respect to magnetic field.

### 1. *Weak localization*

Figure 11(a) shows the low-field MR of the two $\simeq1.3$-$\mu$m wires at 1.25 K, along with data from their codeposited long wire. This figure demonstrates the most striking effect of the probes on the weak-localization MR of the short wires. The magnitude of the MR of both short wires is reduced in comparison to that of the long wire. The MR of the short wire with narrow probes is about half that of the long wire, and the MR of the short wire with wide probes is less than a tenth. $l_\phi$ for these wires at this temperature is 2.39 $\mu$m, as determined by fitting the low-field MR of the codeposited long wire to Eq. (16). From Eqs. (16) and (17), we expect the MR of the short wires to be reduced with respect to the MR of the corresponding long wire. For the short wire with two narrow probes of width $W$ on either end, $\eta=2\alpha$, so that the MR should be reduced by a factor of 2. This is precisely what is seen in Fig. 11(a). For the short wire with wide probes, $\eta$ is larger still, leading to a greater reduction.

At higher temperatures, where $L\gg l_\phi$, we expect the magnitude of the MR of all three wires to be approximately the same. Figure 11(b) shows data for the same three wires at 15 K, where $l_\phi=0.29$ $\mu$m. All three curves are of the same magnitude.

We now turn to another striking effect of the probes on weak localization in short wires. Figure 12 shows the symmetrized low-field MR of sample $B$, the $\simeq 1.3$-$\mu$m wire with wide probes, at 3.5 K. $l_\phi$ at this temperature, as determined from the codeposited long wire, is 1.32 $\mu$m, so that we are in the regime $L/l_\phi \simeq 1$. Note the sharp rise in the MR near zero magnetic field. It should be recalled that a similar feature is seen in the weak localization MR of macroscopic 2D films. Indeed, this feature in the MR of the short wire is due to the influence of the adjacent 2D probes. Figure 12 also shows a fit to the weak-localization formula appropriate for the geometry of sample $B$, Eq. (15). This fit accounts nicely for the sharp rise in the MR. For comparison, we also show the best fit to the formula appropriate for a short wire with narrow probes. By adjusting the value of $l_\phi$ in this formula, we can account for the reduced magnitude of the MR of sample $B$, but we cannot fit the characteristic rise in the MR at low fields.

The 2D nature of the MR in Fig. 12 is not due to an inadvertent inclusion of the 2D probes in the measured sample, because the four-terminal nature of the measurement ensures that we measure only the wire between the probes. If we tried to fit the data for the short wire with wide probes to a sum of pure 1D and pure 2D magnetoresistances, we would have to assume that 90% of the total measured resistance of the sample is due to the 2D measurement probes. Even then, the fit is not good. Since it is safe to assume that the majority of the measured resistance of the sample is due to the short wire itself (due to the four-point nature of the measurement), this possibility can be discounted.

For short samples with only narrow probes, the effect of measurement probes on the shape of the MR is a bit more subtle. When all the measurement probes are of the same width as the sample itself, the shape of the MR is identical to that of the long wire, although the magnitude of the MR may be reduced by a factor as large as the number of probes on one end of the wire. This is because the field dependence of $\eta$ is the same as the field dependence of $\alpha$; the field dependences of both parameters comes through the field dependence of $l_\phi(B)$, which is given by Eq. (18) with the same value of $W$ for both wire and probes. When the width of the probes $W_p$ is different from the width of the wire $W$, the field dependences of $\alpha$ and $\eta$ are no longer identical.

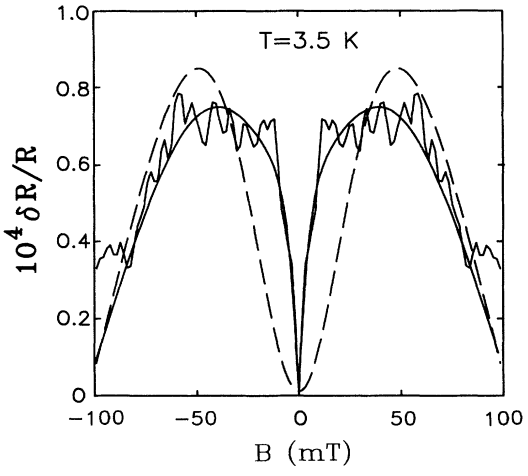


FIG. 12. Symmetric component of the experimental low-field magnetoresistance of sample $B$, a 1.36-$\mu$m wire with wide probes, at 3.5 K. Solid line, fit to the full theory, Eq. (15) with $\eta_2$ defined by Eq. (19) and $l_\phi = 1.3$ $\mu$m, $l_{so} = 0.43$ $\mu$m. Dashed line, fit to the full theory appropriate for a short wire with narrow probes, with $l_\phi = 0.7$ $\mu$m and $l_{so} = 0.46$ $\mu$m.

### 2. *Electron phase coherence lengths in short wires*

We have seen that measurement probes affect both the magnitude and the shape of the low-field MR of short wires, and that with the formulas we derived we are able to fit the MR data quite well. The free parameter in these fits is $l_\phi$, and a further check on the theory is to compare the values of $l_\phi$ obtained to those inferred from the codeposited long wires. This is important because in some cases, one may also be able to fit the MR data for a short wire with the long-wire formula, but with a different value of $l_\phi$. For example, for the short wire with four narrow measurement probes, in the limit $L \ll l_\phi$, the long-wire formula with half the "correct" value of $l_\phi$ will give a reasonable fit.

Values of $l_\phi$ for all four wires, the two wires with wide probes (samples $B$ and $D$) and the two wires with narrow probes ($A$ and $C$) can be conveniently represented on a single plot by scaling the length of each sample with $l_\phi$ inferred from its codeposited long wire, which we shall denote $l_\phi^{\text{long wire}}$. These data are shown in Fig. 13 on a log-log plot. On this plot, data for the long wires are, by definition, straight lines with slope $-1$. The values of $l_\phi$ for sample $C$ in this plot have been normalized to the $R_\square$ and $W$ of the long wire, sample $E$, assuming that the electron-electron scattering rate at low temperatures is determined by scattering off electromagnetic fluctuations.[33] Data for sample $B$, the 1.4-$\mu$m wire with wide probes, could not be fit at the two lowest temperature due to the presence of conductance fluctuations. As can be seen, the agreement with $l_\phi^{\text{long wire}}$ for all four short wires is excellent. We also show the values of $l_\phi$ inferred for the $L = 4.8$-$\mu$m wire with wide probes, sample $D$, using the long-wire formula. For this wire, since $L \gg l_\phi$ at all temperatures measured, the 2D characteristic of the pads is not as prominent, and fits to the long-wire MR formula are reasonable. Nonetheless, the values so obtained are smaller than $l_\phi^{\text{long wire}}$ even for $L \simeq l_\phi^{\text{long wire}}$.

### 3. *Conductance fluctuations*

Although there have been a number of studies on the effect of probes on conductance fluctuations, there has been no investigation of the comparative effects of probes of different size. From both the theoretical discussion on conductance fluctuations given earlier, and the experimental data on weak localization shown above, we expect

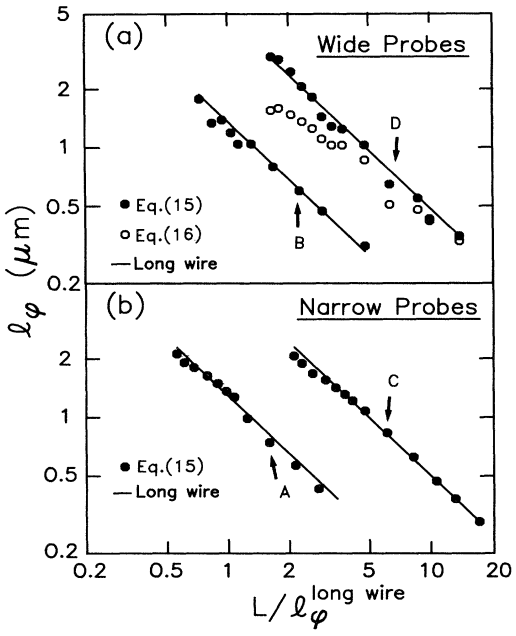


FIG. 13. Experimental $l_\phi$ vs $L/l_\phi^{\text{long wire}}$ for $T=1.25$–$20$ K. Solid lines, with slope $-1$, are data for long wires, samples $E$ and $F$. (a) Data for short wires with wide probes, samples $B$ and $D$. Solid circles from fits to full theory, Eq. (15); open circles from fits to long-wire formula, Eq. (16). (b) Data for short wires with narrow probes, samples $A$ and $C$. Solid circles from fits to Eq. (15). Data for sample $C$ have been normalized to the $R_\square$ and $W$ of sample $E$, as discussed in the text.

that samples with larger measurement probes should show a smaller amplitude of conductance fluctuations. This is indeed the case. Figure 14 shows the rms amplitude of the conductance fluctuations as a function of the length of the sample normalized to $l_\phi$, for the samples with narrow probes and the samples with wide probes discussed above. At large $L/l_\phi$, the amplitude of the fluctuations for both types of sample is approximately the same. As $L/l_\phi \to 0$, however, the amplitude of the fluctuations for the samples with narrow probes becomes larger than that for the samples with wide probes. Unfortunately, the data are in the high-temperature regime ($l_T \ll l_\phi$), so that a detailed quantitative comparison to the theory we have developed is not possible. Nonetheless, the trend in the data is quite clear: smaller probes lead to a larger amplitude of the fluctuations. We expect this trend to continue into the low-temperature regime.

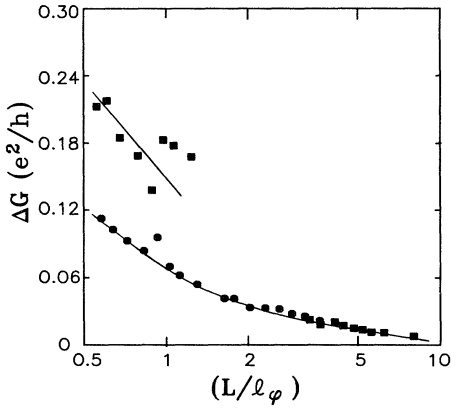


FIG. 14. Experimental rms amplitude of the conductance fluctuations for the short Ag wires as a function of $L/l_\phi^{\text{long wire}}$. Rectangles, data for the short wires with narrow probes, samples $A$ and $C$; circles, data for the short wires with wide probes, samples $B$ and $D$. The solid lines are guides to the eye. The lengths of the short wires with narrow probes were such that the data did not fall into the intermediate length regime.

## IV. CONCLUSIONS

Weak localization has been studied now for over a decade. Only with the advent of more quantitative theories could localization be used as a tool to study other problems in the physics of disordered systems. Some of these problems are quite difficult to address by any other means. The study of weak localization in three-, two-, and one-dimensional systems has been used with great success to infer various useful microscopic scattering lengths $l_\phi$, $l_{so}$, and $l_s$ for electron transport in metallic structures. In these cases, at least one of the sample dimensions is much larger than any of the microscopic scattering lengths. It is useful to investigate electron-scattering mechanisms in the regime where all the dimensions of the sample are comparable to or less than the relevant microscopic length scale. To do this, one requires a means of inferring electron-scattering lengths from data on samples in the mesoscopic size regime.

This paper provides a quantitative theory of weak localization for mesoscopic samples. The theory is applicable to short wires with virtually any probe configuration, and the formalism we have developed can be extended easily to more complicated sample geometries. The agreement with experimental results is excellent. The phase coherence lengths obtained by fitting weak-localization data from mesoscopic samples to this theory are consistent with the phase coherence lengths obtained from earlier studies on macroscopic films and wires. Thus we now have a means of determining electron phase coherence lengths in the mesoscopic size regime.

In addition, we have found it appealing that the effect of probes can be seen directly in the magnetoresistance due to weak localization. The physical insight one develops in such a study has been valuable in our study of conductance fluctuations. For example, we point out the analogy between weak-localization magnetoresistance and the magnetic-field autocorrelation function for the conductance fluctuations. By examining the simpler case of weak localization, one can make qualitative predictions about the more complicated case of conductance fluctuations.

In some cases, the low-field weak-localization magnetoresistance is either absent (as would be the case if the sample had magnetic impurities) or is masked by much larger conductance fluctuations. Instead of weak localization, one could then hope to use the conductance fluc-

tuations themselves to determine the electron phase coherence length, by fitting the measured correlation function to theoretical predictions. Unfortunately, we cannot make quantitative predictions for conductance fluctuations for an arbitrary sample geometry. So far, because the mathematics becomes intimidating as one goes to complicated geometries, we can make predictions for only the simplest cases. This is not necessarily a restriction. We do, after all, have predictions in closed form for four-probe 1D wire with 1D probes of any width, and one can always make a sample in this configuration. Perhaps a greater restriction is that all the multiprobe theories for fluctuations that we are aware of, including ours, deal only with the low-temperature regime $l_T \gg l_\phi$. Very few metallic samples actually fall into this regime. Only if the electron phase coherence length saturates at low temperatures (due to the presence of paramagnetic impurities at low magnetic fields) will the sample be in the low-temperature regime.

Thus much more work needs to be done to obtain a quantitative multiprobe theory for conductance fluctuations which is valid in all temperature regimes. Why is there a need for such a theory? As we have pointed out, one could then use conductance fluctuations much in the way one uses weak localization, as a tool to determine phase coherence lengths in regimes where weak localization is absent. However, as pointed out in Sec. II B 1, there is the interesting possibility that the phase coherence that determines conductance fluctuations may be more robust than the phase coherence responsible for weak localization. There appears to be some experimental evidence[34] in support of this, although a thorough study is required and such a study needs a quantitative multiprobe theory of conductance fluctuations in the high-temperature regime.

## ACKNOWLEDGMENTS

We thank B. Douçot, D. P. DiVincenzo, B. L. Altshuler, A. D. Stone, S. Sachdev, and N. Read for useful discussions, and S. J. Klepper, M. J. Rooks, and S. Wind for assistance in the experiments. We thank R. A. Webb and S. Washburn for discussions related to and for the use of their data in Figs. 9 and 10, respectively. Research at Yale University was supported by the NSF Grant No. DMR-8505539.

## APPENDIX: TWO-DIMENSIONAL PROBES IN A MAGNETIC FIELD

Let the plane of the 2D film be in the $r,\theta$ plane in the cylindrical coordinate system, with the magnetic field $\mathbf{B}=B\hat{\mathbf{z}}$. In the cylindrical gauge $\mathbf{A}=(Br/2)\hat{\boldsymbol{\theta}}$, the homogeneous part of Eq. (6) becomes[35]

$$\left[-\frac{1}{r}\frac{\partial}{\partial r}\left[r\frac{\partial}{\partial r}\right]+\left[\frac{eB}{\hbar}\right]^2 r^2-\frac{1}{r^2}\frac{\partial^2}{\partial\theta^2}+2i\left[\frac{eB}{\hbar}\right]+\frac{1}{l_{\phi 2D}^2}\right]C(\mathbf{r},\mathbf{r}')=0 . \quad \text{(A1)}$$

Consider solutions of the form

$$C(r,\theta)=(1/2\pi)^{1/2}R(r)e^{im\theta} . \quad \text{(A2)}$$

We are interested in solutions with $m=0$. The equation for $R(r)$ then becomes

$$\left[\frac{d^2}{dr^2}+\frac{1}{r}\frac{d}{dr}-\left[\frac{eB}{\hbar}\right]^2 r^2-\frac{1}{l_{\phi 2D}^2}\right]R(r)=0 . \quad \text{(A3)}$$

Making the transformation $\xi=(eB/\hbar)r^2$ and writing $R(\xi)=w(\xi)\exp(-\xi/2)$, we obtain the equation for $w(\xi)$,

$$\left[\xi\frac{d^2}{d\xi^2}+(1-\xi)\frac{d}{d\xi}-\left[\frac{1}{2}+\frac{B_\phi}{B}\right]\right]w(\xi)=0 , \quad \text{(A4)}$$

where $B_\phi=\hbar/4el_{\phi 2D}^2$. The general solution is in terms of confluent hypergeometric functions[35]

$$w(\xi)=C\Phi[\tfrac{1}{2}+(B_\phi/B),1;\xi]+D\Psi[\tfrac{1}{2}+(B_\phi/B),1;\xi] , \quad \text{(A5)}$$

where $C$ and $D$ are constants. Since $\Phi\to 0$ as $\xi\to 0$, we set $C=0$. The solution to Eq. (A1) is

$$C(\mathbf{r},\mathbf{r}')=D\exp[-(eB/2\hbar)r^2]\times\Psi[\tfrac{1}{2}+(B_\phi/B),1;(eB/\hbar)r^2] . \quad \text{(A6)}$$

To determine $D$, we must specify the boundary conditions. We would like to specify the boundary condition at $r=0$ since this will be useful for writing the node equations. However, $\Psi$ diverges as $r\to 0$. This is familiar in the calculation of the 2D weak-localization magnetoresistance. There the problem is avoided by introducing a cutoff in the $q$ space at $1/l$. In real space this is equivalent to specifying the boundary condition at $r=l$. Setting $C(\mathbf{r},\mathbf{r}')=C_a$ at $r=l$, we have

$$C_a=D\exp(-2B/B_0)\Psi[\tfrac{1}{2}+(B_\phi/B),1;(B/4B_0)] . \quad \text{(A7)}$$

Since $(B/4B_0)$ is small we can take the small argument of the $\Psi$ function, and equate the exponential to unity to obtain

$$D=-\frac{C_a\Gamma[\frac{1}{2}+(B_\phi/B)]}{\ln(B/4B_0)+\psi[\frac{1}{2}+(B_\phi/B)]} . \quad \text{(A8)}$$

$\Gamma$ is the gamma function and $\psi$ is the digamma function.

To determine the constant $\eta_2$ in Eq. (14a), we need $\lim_{r\to 0}(d/dr)C(r,r')$. Further note that

$$\lim_{z\to 0}\Psi'(x,1;z)=-[x\Gamma(1)/\Gamma(x+1)z]$$

and hence we obtain

$$\lim_{r\to 0}\frac{d}{dr}C(r,r')=\frac{2C_a}{r\{\ln(B/4B_0)+\psi[\frac{1}{2}+(B_\phi/B)]\}} . \quad \text{(A9)}$$

As $B\to 0$ this becomes $-C_a/[r\ln(2l_{\phi 2D}/l)]$. The parameter $\eta_2$ is obtained from this by integrating over the angular coordinate which in our approximation is equivalent to multiplying by $r\theta$, the length of the arc at radius $r$.

[1]S. Washburn and R. A. Webb, Adv. Phys. **35**, 375 (1986).
[2]P. A. Lee, A. D. Stone, and H. Fukuyama, Phys. Rev. B **35**, 1039 (1987).
[3]A. Benoit, C. P. Umbach, R. B. Laibowitz, and R. A. Webb, Phys. Rev. Lett. **58**, 2343 (1987).
[4]W. J. Skocpol, P. M. Mankiewich, R. E. Howard, L. D. Jackel, D. M. Tennant, and A. D. Stone, Phys. Rev. Lett. **58**, 2347 (1987).
[5]B. L. Altshuler, Pis'ma Zh. Eksp. Teor. Fiz. **41**, 530 (1985) [JETP Lett. **41**, 648 (1985)].
[6]P. A. Lee and A. D. Stone, Phys. Rev. Lett. **55**, 1622 (1985).
[7]A. Benoit, S. Washburn, C. P. Umbach, R. B. Laibowitz, and R. A. Webb, Phys. Rev. Lett. **57**, 1765 (1986).
[8]M. Büttiker, Phys. Rev. Lett. **57**, 1761 (1986); Phys. Rev. B **35**, 4123 (1987).
[9]R. A. Serota, Shechao Feng, C. Kane, and P. A. Lee, Phys. Rev. B **36**, 5031 (1987).
[10]S. Maekawa, Y. Isawa, and H. Ebisawa, J. Phys. Soc. Jpn. **56**, 25 (1987).
[11]H. U. Baranger, A. D. Stone, and D. P. DiVincenzo, Phys. Rev. B **37**, 6521 (1988).
[12]C. L. Kane, P. A. Lee, and D. P. DiVincenzo, Phys. Rev. B **38**, 2995 (1988).
[13]D. P. DiVincenzo and C. L. Kane, Phys. Rev. B **38**, 3006 (1988).
[14]S. Hershfield and V. Ambegaokar, Phys. Rev. B **38**, 7909 (1988).
[15]G. Bergmann, Phys. Rep. **107**, 1 (1984).
[16]B. L. Altshuler, A. G. Aronov, D. E. Khmel'nitskii, and A. I. Larkin, in *Quantum Theory of Solids,* edited by I. M. Lifshitz (MIR, Moscow, 1982).
[17]V. Chandrasekhar, M. J. Rooks, S. Wind, and D. E. Prober, Phys. Rev. Lett. **55**, 1610 (1985); V. Chandrasekhar, Ph. D. thesis, Yale University, 1989 (available from University Microfilms, Ann Arbor, MI 48106).
[18]B. L. Altshuler, A. G. Aronov, and B. Z. Spivak, Pis'ma Zh. Eksp. Teor. Fiz. **33**, 101 (1981) [JETP Lett. **33**, 94 (1981)].
[19]V. Chandrasekhar, D. E. Prober, and P. Santhanam, Phys. Rev. Lett. **61**, 2253 (1988).
[20]B. L. Altshuler, A. G. Aronov, and A. Yu. Zyuzin, Zh. Eksp. Teor. Fiz. **86**, 709 (1984) [Sov. Phys. JETP **59**, 415 (1984)]; P. Santhanam, Phys. Rev. B **35**, 8737 (1987).
[21]B. Douçot and R. Rammal, Phys. Rev. Lett. **55**, 1148 (1985); J. Phys. (Paris) **47**, 973 (1986).
[22]S. Wind, M. J. Rooks, V. Chandrasekhar, and D. E. Prober, Phys. Rev. Lett. **57**, 633 (1986); J. J. Lin and N. Giordano, Phys. Rev. B **33**, 1519 (1986); K. Ishibashi, K. Gamo, S. Namba, S. Ishida, and K. Murase, Solid State Commun. **58**, 743 (1986).
[23]B. L. Altshuler and A. G. Aronov, Pis'ma Zh. Eksp. Teor. Fiz. **33**, 515 (1981) [JETP Lett. **33**, 499 (1981)].
[24]A. H. Verbruggen, H. Vloeberghs, P. A. M. Holweg, C. Van Haesendonck, S. Radelaar, and Y. Bruynseraede, in *Nanostructures: Fabrication and Physics,* Proceedings of the Materials Research Society Meeting, Boston, 1990, edited by S. D. Berger, H. G. Craighead, D. Kern, and T. P. Smith III (Materials Research Society, Pittsburgh, 1990).
[25]P. Santhanam, Phys. Rev. B **39**, 2541 (1989).
[26]D. E. Khmelnitskii, Physica B **126**, 235 (1984).
[27]C. W. J. Beenakker and H.van Houten, Phys. Rev. B **37**, 6544 (1988).
[28]H. Haucke, S. Washburn, A. D. Benoit, C. P. Umbach, and R. A. Webb, Phys. Rev. B **41**, 12 454 (1990).
[29]O. Millo, S. J. Klepper, M. W. Keller, D. E. Prober, S. Xiong, A. D. Stone, and R. N. Sacks, Phys. Rev. Lett. **65**, 1494 (1990); V. Chandrasekhar, P. Santhanam, and D. E. Prober, Phys. Rev. B **42**, 6823 (1990).
[30]J. T. Masden and N. Giordano, Phys. Rev. Lett. **49**, 819 (1982).
[31]K. K. Choi, D. C. Tsui, and S. C. Palmateer, Phys. Rev. B **33**, 8216 (1986).
[32]D. J. Bishop and G. J. Dolan, Phys. Rev. Lett. **55**, 2911 (1985).
[33]B. L. Altshuler, A. G. Aronov, and D. E. Khmelnitskii, J. Phys. C **15**, 7367 (1982).
[34]R. A. Webb (private communication).
[35]L. P. Landau and I. M. Lifshitz, *Quantum Mechanics (Non-relativistic Theory)* (Pergamon, New York, 1980); N. N. Lebedev, *Special Functions and Their Applications* (Dover, New York, 1972).